GEOPHYSICS, VOL. 66, NO. 4 (JULY-AUGUST 2001); P. 1258–1266, 7 FIGS., 2 TABLES.

The application of the perfectly matched layer in numerical modeling of wave propagation in poroelastic media

Y. Q. Zeng, J. Q. He, and Q. H. Liu*

ABSTRACT

The perfectly matched layer (PML) was first introduced by Berenger as a material absorbing boundary condition (ABC) for electromagnetic waves. In this paper, a method is developed to extend the perfectly matched layer to simulating seismic wave propagation in poroelastic media. This nonphysical material is used at the computational edge of a finite-difference algorithm as an ABC to truncate unbounded media. The incorporation of PML in Biot's equations is different from other PML applications in that an additional term involving convolution between displacement and a loss coefficient in the PML region is required. Numerical results show that the PML ABC attenuates the outgoing waves effectively.

INTRODUCTION

Elastic wave propagation in a poroelastic medium is governed by Biot's theory (Biot, 1956a, b, 1962a, b). In a homogeneous medium, analytical solutions for Biot's equations can be obtained easily, but such solutions are in general impossible for an arbitrary heterogeneous medium. Elastic wave propagation in complex poroelastic media is of great interest in geophysics and other branches of applied sciences, such as petroleum engineering, structure mechanics, and seismology. Numerical methods are usually employed to solve these problems. Examples of numerical methods include the finite-difference, finite element, and pseudospectral methods. In this paper, a finite-difference method will be used.

In numerical simulation of wave propagation in an unbounded medium, the imposition of artificial boundaries introduces spurious reflections which will affect the accuracy of numerical solutions. Although the problem can be overcome by increasing the size of the model, it is not always feasible because of the large amount of computer memory required for long-time solutions. It is thus highly desirable to eliminate these reflections by using absorbing boundary conditions (ABCs) when simulating an unbounded medium. Developing an effective and stable ABC is always one of the most important tasks in numerical modeling of wave propagation. Smith (1974) proposed an ABC for finite-difference and finite element methods. In his method, the Dirichlet and Neumann conditions are used alternatively, and the solutions from these two conditions are superimposed. Although easy to implement, this method greatly increases the computation time. A widely used ABC in seismic modeling proposed by Clayton and Engquist (1977) is the one-way wave equation based on the paraxial approximations of the acoustic or elastic equations. Similar approaches were proposed by several authors, including Reynolds (1978). Although effective for small incidence angles, these absorbing boundary conditions degrade for large angles of incidence. Furthermore, they are known to have instability problem when the Poisson's ratio is greater than 2.0 (Mahrer, 1986; Stacey, 1988). Another approach is to add a spatial filter or damping taper to the boundaries (Cerjan et al., 1985; Kosloff and Kosloff, 1986). In this so-called sponge absorber method, the transition zone from the inner region to the outer boundary should be thick and smooth. Liao et al. (1984) developed an ABC based on the principle of plane wave and interpolation. Although effective even for perpendicular inhomogeneous boundary intersecting the absorbing boundary, Liao's ABC requires double precision for stability.

In 1994, Berenger proposed a highly effective perfectly matched layer (PML) as an absorbing boundary condition for electromagnetic waves. It has since been widely used for finite-difference and finite element methods (e.g., Chew and Weedon, 1994; Liu, 1997). Chew and Liu (1996) first proved that such a perfectly matched layer also exists for elastic waves in spite of the coupling of *S*- and *P*-waves at an elastic interface. In the continuous limit, the PML has zero reflection to the regular elastic medium, although a small reflection can result from discretization in the PML scheme. Hastings et al. (1996) independently implemented the PML ABC for two-dimensional problems using potentials. The PML ABC has also been extended to model acoustic waves and electromagnetic waves in

Manuscript received by the Editor August 6, 1999; revised manuscript received November 30, 2000.
*Duke University, Department of Electrical Engineering, 130 Hudson Hall, Box 90291, Durham, North Carolina 27708-0291. E-mail: yz3@ee.duke.edu; Qing.Liu@ee.duke.edu; jhe@ee.duke.edu.

lossy media (Liu, 1997; Liu and Tao, 1997) as well as electromagnetic and elastic waves in cylindrical and spherical coordinates (Liu, 1999; He and Liu, 1999).

These previous ABCs, however, have been developed for electromagnetic, acoustic, and elastic waves in solids. Little attention has been paid to elastic waves in porous media. In this work, we extend the PML to truncate unbounded poroelastic media for numerical solutions using a finite-difference method. We adopt the method of complex coordinates (Chew and Weedon, 1994; Liu, 1997; Liu and Tao, 1997) to formulate the PML for poroelastic media. Two-dimensional finite-difference results show the efficiency of the PML ABC.

PROBLEM FORMULATION

Biot's theory for elastic waves in porous media was established on a macroscopic level (Biot, 1956a, b, 1962a, b). The anelastic effects arise from viscous interactions between the fluid and the solid matrix. The following assumptions are used in the theory: (1) seismic wavelength is large in comparison to the pore size, (2) the deformations are small, (3) the liquid phase is continuous, such that pores are connected and the disconnected pores are part of the matrix, (4) the solid matrix is elastic, (5) the medium is statistically isotropic, and (6) gravity forces are neglected. At low frequency, wave propagation in a heterogeneous, porous medium is described by following equations:

$$2\sum_j \frac{\partial}{\partial x_j}(\mu e_{ij}) + \frac{\partial}{\partial x_i}(\lambda_c e - \alpha M \xi) = \frac{\partial^2}{\partial t^2}(\rho u_i + \rho_f w_i), \tag{1}$$

$$\frac{\partial}{\partial x_i}(\alpha M e - M\xi) = \frac{\partial^2}{\partial t^2}(\rho_f u_i + m w_i) + \frac{\eta}{\kappa}\frac{\partial w_i}{\partial t}, \tag{2}$$

where $m = a\rho_f/\phi$ and

$$M = \left(\frac{\phi}{K_f} + \frac{\alpha - \phi}{K_s}\right)^{-1},$$
$$\alpha = 1 - \frac{K_b}{K_s}.$$

In these equations, the parameters describing the physical properties of the medium are as follows: μ = shear modulus of dry porous matrix, λ_c = Lame constant of saturated matrix, ϕ = porosity, η = viscosity, κ = permeability, ρ = the overall density of the saturated medium determined by $\rho_f\phi + (1-\phi)\rho_s$, ρ_s = density of solid material, ρ_f = density of fluid, a = tortuosity of the matrix, K_s = bulk modulus of the solid, K_f = bulk modulus of the fluid, and K_b = bulk modulus of the dry porous frame.

In equations (1) and (2), $i, j = 1, 2, 3$; u_i is the ith component of the displacement vector of the solid material and $w_i = \phi(U_i - u_i)$ is the ith component of the displacement vector of the pore fluid relative to that of the solid, U_i is the displacement vector of the pore fluid, $e = \nabla \cdot \mathbf{u}$ is the dilatation for the solid motion, $\xi = -\nabla \cdot \mathbf{w}$ is the dilatation for the relative motion between the fluid and the solid, and $e_{ij} = [(\partial u_j/\partial x_i + \partial u_i/\partial x_j)/2]$, is the strain tensor in the porous medium. In Cartesian coordinates, x_1, x_2 and x_3 are equivalent to x, y and z.

In a two-dimensional XZ plane, equations (1) and (2) can be reorganized as

$$\begin{aligned}(m\rho - \rho_f^2)\frac{\partial^2 u_1}{\partial t^2} &= 2m\frac{\partial}{\partial x_1}\left(\mu\frac{\partial u_1}{\partial x_1}\right) + m\frac{\partial}{\partial x_2}\left(\mu\frac{\partial u_1}{\partial x_2}\right) \\ &+ m\frac{\partial}{\partial x_2}\left(\mu\frac{\partial u_2}{\partial x_1}\right) + m\frac{\partial}{\partial x_1}\left(\lambda_c\frac{\partial u_1}{\partial x_1}\right) \\ &+ m\frac{\partial}{\partial x_1}\left(\lambda_c\frac{\partial u_2}{\partial x_2}\right) + m\frac{\partial}{\partial x_1}\left(\alpha M\frac{\partial w_1}{\partial x_1}\right) \\ &+ m\frac{\partial}{\partial x_1}\left(\alpha M\frac{\partial w_2}{\partial x_2}\right) - \rho_f\frac{\partial}{\partial x_1}\left(\alpha M\frac{\partial u_1}{\partial x_1}\right) \\ &- \rho_f\frac{\partial}{\partial x_1}\left(\alpha M\frac{\partial u_2}{\partial x_2}\right) - \rho_f\frac{\partial}{\partial x_1}\left(M\frac{\partial w_1}{\partial x_1}\right) \\ &- \rho_f\frac{\partial}{\partial x_1}\left(M\frac{\partial w_2}{\partial x_2}\right) + \rho_f\frac{\eta}{\kappa}\frac{\partial w_1}{\partial t}, \end{aligned} \tag{3}$$

$$\begin{aligned}(m\rho - \rho_f^2)\frac{\partial^2 w_1}{\partial t^2} &= \rho\frac{\partial}{\partial x_1}\left(\alpha M\frac{\partial u_1}{\partial x_1}\right) + \rho\frac{\partial}{\partial x_1}\left(\alpha M\frac{\partial u_2}{\partial x_2}\right) \\ &+ \rho\frac{\partial}{\partial x_1}\left(M\frac{\partial w_1}{\partial x_1}\right) + \rho\frac{\partial}{\partial x_1}\left(M\frac{\partial w_2}{\partial x_2}\right) \\ &+ 2\rho_f\frac{\partial}{\partial x_1}\left(\mu\frac{\partial u_1}{\partial x_1}\right) - \rho_f\frac{\partial}{\partial x_2}\left(\mu\frac{\partial u_1}{\partial x_2}\right) \\ &- \rho_f\frac{\partial}{\partial x_2}\left(\mu\frac{\partial u_2}{\partial x_1}\right) - \rho_f\frac{\partial}{\partial x_1}\left(\lambda_c\frac{\partial u_1}{\partial x_1}\right) \\ &- \rho_f\frac{\partial}{\partial x_1}\left(\lambda_c\frac{\partial u_2}{\partial x_2}\right) - \rho_f\frac{\partial}{\partial x_1}\left(\alpha M\frac{\partial w_1}{\partial x_1}\right) \\ &- \rho_f\frac{\partial}{\partial x_1}\left(\alpha M\frac{\partial w_2}{\partial x_2}\right) - \rho\frac{\eta}{\kappa}\frac{\partial w_1}{\partial t}, \end{aligned} \tag{4}$$

$$\begin{aligned}(m\rho - \rho_f^2)\frac{\partial^2 u_2}{\partial t^2} &= m\frac{\partial}{\partial x_1}\left(\mu\frac{\partial u_2}{\partial x_1}\right) + m\frac{\partial}{\partial x_1}\left(\mu\frac{\partial u_1}{\partial x_2}\right) \\ &+ 2m\frac{\partial}{\partial x_2}\left(\mu\frac{\partial u_2}{\partial x_2}\right) + m\frac{\partial}{\partial x_2}\left(\lambda_c\frac{\partial u_1}{\partial x_1}\right) \\ &+ m\frac{\partial}{\partial x_2}\left(\lambda_c\frac{\partial u_2}{\partial x_2}\right) + m\frac{\partial}{\partial x_2}\left(\alpha M\frac{\partial w_1}{\partial x_1}\right) \\ &+ m\frac{\partial}{\partial x_2}\left(\alpha M\frac{\partial w_2}{\partial x_2}\right) - \rho_f\frac{\partial}{\partial x_2}\left(\alpha M\frac{\partial u_1}{\partial x_1}\right) \\ &- \rho_f\frac{\partial}{\partial x_2}\left(\alpha M\frac{\partial u_2}{\partial x_2}\right) - \rho_f\frac{\partial}{\partial x_2}\left(M\frac{\partial w_1}{\partial x_1}\right) \\ &- \rho_f\frac{\partial}{\partial x_2}\left(M\frac{\partial w_2}{\partial x_2}\right) + \rho_f\frac{\eta}{\kappa}\frac{\partial w_2}{\partial t}, \end{aligned} \tag{5}$$

and

$$\begin{aligned}(m\rho - \rho_f^2)\frac{\partial^2 w_2}{\partial t^2} &= \rho\frac{\partial}{\partial x_2}\left(\alpha M\frac{\partial u_1}{\partial x_1}\right) + \rho\frac{\partial}{\partial x_2}\left(\alpha M\frac{\partial u_2}{\partial x_2}\right) \\ &+ \rho\frac{\partial}{\partial x_2}\left(M\frac{\partial w_1}{\partial x_1}\right) + \rho\frac{\partial}{\partial x_2}\left(M\frac{\partial w_2}{\partial x_2}\right) \\ &- \rho_f\frac{\partial}{\partial x_1}\left(\mu\frac{\partial u_2}{\partial x_1}\right) - \rho_f\frac{\partial}{\partial x_1}\left(\mu\frac{\partial u_1}{\partial x_2}\right) \\ &- 2\rho_f\frac{\partial}{\partial x_2}\left(\mu\frac{\partial u_2}{\partial x_2}\right) - \rho_f\frac{\partial}{\partial x_2}\left(\lambda_c\frac{\partial u_1}{\partial x_1}\right) \\ &- \rho_f\frac{\partial}{\partial x_2}\left(\lambda_c\frac{\partial u_2}{\partial x_2}\right) - \rho_f\frac{\partial}{\partial x_2}\left(\alpha M\frac{\partial w_1}{\partial x_1}\right) \\ &- \rho_f\frac{\partial}{\partial x_2}\left(\alpha M\frac{\partial w_2}{\partial x_2}\right) - \rho\frac{\eta}{\kappa}\frac{\partial w_2}{\partial t}. \end{aligned} \tag{6}$$

We aim to solve these equations numerically for the displacement fields in an unbounded medium. To this end, we first formulate the PML as the absorbing boundary condition.

Complex coordinates for absorptive media

In order to introduce the PML for seismic waves in absorptive media, equations (1) and (2) will be modified using the complex stretched coordinates. In the frequency domain, the complex coordinate-stretching variable is chosen as

$$\tilde{x}_j = \int_0^{x_j} e_{x_j}(x_j)\,dx_j, \quad e_{x_j} = a_{x_j} + i\frac{\omega_{x_j}}{\omega} \quad (j=1,2,3), \tag{7}$$

where $i=\sqrt{-1}$, $a_{x_j} \geq 1$ and $\omega_{x_j} \geq 0$.

In the PML formulation, the regular coordinate variable x_j is replaced by the complex coordinate variable $\tilde{x}_j$. The derivative $\partial/\partial\tilde{x}_j$ can be expressed in terms of the complex coordinate-stretching variables

$$\frac{\partial}{\partial\tilde{x}_j} = \frac{1}{e_{x_j}}\frac{\partial}{\partial x_j} \quad (j=1,2,3), \tag{8}$$

where a time dependence of $e^{-i\omega t}$ is implied. In equation (7), for a PML region, the real part a_{x_j} is a scaling factor, and the imaginary part ω_{x_j} represents a loss in the PML. In a regular non-PML region, $a_{x_j}=1$ and $\omega_{x_j}=0$. Replacing the spatial derivatives in equations (3)–(6) with those in terms of complex coordinates, we arrive at the frequency domain wave equations for porous medium. In particular, equations (1) and (2) become in complex coordinates

$$2\sum_j \frac{\partial}{\partial\tilde{x}_j}(\mu e_{ij}) + \frac{\partial}{\partial\tilde{x}_i}(\lambda_c e - \alpha M\xi) = \frac{\partial^2}{\partial t^2}(\rho u_i + \rho_f w_i), \tag{9}$$

$$\frac{\partial}{\partial\tilde{x}_i}(\alpha M e - M\xi) = \frac{\partial^2}{\partial t^2}(\rho_f u_i + m w_i) + \frac{\eta}{\kappa}\frac{\partial w_i}{\partial t}. \tag{10}$$

The zero reflection of the PML has been proved by Chew and Liu (1996) for elastic media. Their proof was based on the reflection and transmission coefficients at a planar interface between the PML medium and a regular medium. It was later found that this lengthy proof is actually unnecessary (Teixeira and Chew, 1997; Liu, 1999). This is also true for poroelastic media. Indeed, the fact that the PML has zero reflection to the regular poroelastic medium follows the simple observation that equations (9) and (10) have exactly the same form as the original equations (1) and (2). Thus, the same solutions obtained for the regular media can be mapped to the PML media through a simple analytic continuation of the spatial variables to a complex space. This simple method for the construction of PML equations is especially useful for non-Cartesian coordinates (Teixeira and Chew, 1997; He and Liu, 1999; Liu, 1999).

Splitting of equations in time domain

Before incorporating the stretching variables, each of equations (3)–(6) is split into three equations, corresponding to three displacement variables. For example, for the horizontal displacement u_1 of solid, we have

$$u_1 = u_1^a + u_1^b + u_1^c,$$

where

$$u_1^a \sim \frac{\partial}{\partial x_1}\left(g\frac{\partial u_1}{\partial x_1}\right),$$
$$u_1^b \sim \frac{\partial}{\partial x_1}\left(g\frac{\partial u_1}{\partial x_2}\right),$$
$$or\ \frac{\partial}{\partial x_2}\left(g\frac{\partial u_1}{\partial x_1}\right),$$
$$u_1^c \sim \frac{\partial}{\partial x_2}\left(g\frac{\partial u_1}{\partial x_2}\right).$$

Here g represents a function of space. We then transform all equations to the frequency domain with complex coordinates.

Applying these schemes to equations (3)–(6), we obtain a total of 12 equations with respect to u_1^a, u_1^b, u_1^c, u_2^a, u_2^b, u_2^c, w_1^a, w_1^b, w_1^c, w_2^a, w_2^b, and w_2^c. For example, for u_1^a, the equation is

$$\begin{aligned}
\rho_f\frac{\eta}{\kappa}(i\omega)w_1^a + (m\rho-\rho_f^2)(-\omega^2)u_1^a = {} & \frac{2m}{e_{x_1}^2}\left[-\frac{e'_{x_1}}{e_{x_1}}\left(\mu\frac{\partial u_1}{\partial x_1}\right) + \frac{\partial}{\partial x_1}\left(\mu\frac{\partial u_1}{\partial x_1}\right)\right] + \frac{m}{e_{x_1}^2}\left[-\frac{e'_{x_1}}{e_{x_1}}\left(\lambda_c\frac{\partial u_1}{\partial x_1}\right) + \frac{\partial}{\partial x_1}\left(\lambda_c\frac{\partial u_1}{\partial x_1}\right)\right] \\
& + \frac{m}{e_{x_1}^2}\left[-\frac{e'_{x_1}}{e_{x_1}}\left(\alpha M\frac{\partial w_1}{\partial x_1}\right) + \frac{\partial}{\partial x_1}\left(\alpha M\frac{\partial w_1}{\partial x_1}\right)\right] \\
& - \frac{\rho_f}{e_{x_1}^2}\left[-\frac{e'_{x_1}}{e_{x_1}}\left(\alpha M\frac{\partial u_1}{\partial x_1}\right) + \frac{\partial}{\partial x_1}\left(\alpha M\frac{\partial u_1}{\partial x_1}\right)\right] \\
& - \frac{\rho_f}{e_{x_1}^2}\left[-\frac{e'_{x_1}}{e_{x_1}}\left(M\frac{\partial w_1}{\partial x_1}\right) + \frac{\partial}{\partial x_1}\left(M\frac{\partial w_1}{\partial x_1}\right)\right],
\end{aligned} \tag{11}$$

where $e'_{x_1} = i(d\omega_{x_1}/dx_1)/\omega$. Then we transform all these 12 equations back to the time domain. For example, in the time domain, equation (11) becomes

$$\begin{aligned}
-\rho_f\frac{\eta}{\kappa}\left[\frac{\partial w_1^a}{\partial t} + 2\omega_{x_1}w_1^a + \omega_{x_1}^2\int_0^t w_1^a\,d\tau\right] - (m\rho-\rho_f^2) \\
\times\left[-\frac{\partial^2 u_1^a}{\partial t^2} - 2\omega_{x_1}\frac{\partial u_1^a}{\partial t} - \omega_{x_1}^2 u_1^a\right] = R,
\end{aligned} \tag{12}$$

where R is the inverse transformation of the right side of equation (11) times $e_{x_1}^2$. The multiplication of e'_{x_1}/e_{x_1} and $\mu(\partial u_1/\partial x_1)$ in the frequency domain leads to the convolution of these two terms in time domain. Since e'_{x_1}/e_{x_1} is an exponential function in the time domain, this convolution can be obtained efficiently as follows. Let $f(t)$ represent the inverse Fourier transform of $(e'_{x_1}/e_{x_1})\,\mu(\partial u_1/\partial x_1)$. It can be computed via

$$\begin{aligned}
f(t) = e^{-\omega_{x_1}(x_1)\triangle t}\Big[& f(t-\triangle t) + \mu\omega'_{x_1}(x_1) \\
& \int_{t-\triangle t}^{t} e^{-\omega_{x_1}(x)(t-\tau)}\frac{\partial u_1(\tau)}{\partial x_1}\,d\tau\Big].
\end{aligned}$$

This requires the storage of u_1 at $(n-1)$th and nth time steps only. Similar equations can be obtained for u_1^b, u_1^c, and other field components.

It is worthwhile to note that these splittings are only necessary inside the PML region. The number of cells in the PML region is about $2m(N_x+N_z)$, where m is the thickness of the

PML region, and N_x and N_z are the total number of nodes in the x and z directions, respectively. For a large-scale problem, the ratio between this number and the total number of nodes $2m(N_x + N_z)/N_x N_z$ is negligible.

Finite-difference implementation

In the last section, we obtained 12 time-domain equations for 12 split field variables u_1^a, u_1^b, u_1^c, u_2^a, u_2^b, u_2^c, w_1^a, w_1^b, w_1^c, w_2^a, w_2^b, and w_2^c, which already incorporate the PML boundary condition.In numerical implementation, the time and space are discretized by time step $\triangle t$ and node spacing $\triangle x$ and $\triangle z$. The unbounded medium is truncated into a finite computational domain with a total of $N_x \times N_z$ grid nodes. Then, the central finite-difference method is applied to each equation to obtain the updated displacement at next time step. In this FD scheme, both spatial and temporal derivatives are obtained by central differencing. Thus, it is an explicit scheme with second-order accuracy both in spatial and temporal domains.

With the PML boundary condition, the computational domain is partitioned into a regular interior region and the boundary PML region. Unfortunately, the stability condition of the finite-difference method for the PML material does not seem to have a closed-form solution. However, numerical experiments suggest that the stability condition is the same as the regular medium when the damping coefficient $b = \eta/\kappa$ is negligible.

The absorption of outgoing wave is achieved by the PML region, which consists of several cells of PML materials with a quadratically or linearly tapered profile to increase the attenuation toward the outer boundary. In this paper, 20 cells of PML with a quadratic profile for ω_{x_j} are used. So the ω_x and ω_z have the following forms

$$\omega_{x_i} = \begin{cases} 2\pi a_0 f_0 (\ell_{x_i}/L_{PML})^2, & \text{inside PML,} \\ 0, & \text{outside PML,} \end{cases}$$

where f_0 is the dominant frequency of the source described in the next section, L_{PML} is the thickness of the PML cells, and ℓ_{x_i} is the distance from the interface between the interior region and PML region. After testing several values for a_0, we found 1.79 has the best absorption of outgoing waves. The outer boundary conditions for the PML are those for a hard boundary (or alternatively, a soft boundary).

Discussions

The above formulation for the perfectly matched layer is based on the complex coordinates and is a natural extension of our earlier work on PML for acoustic and elastic waves (Chew and Liu, 1996; Liu and Tao, 1997, Liu, 1998, 1999). The novelty of the PML formulation using the complex coordinates is that the governing equations and the solution forms remain identical to those in the regular coordinates. Therefore, in the continuum, the boundary between a PML material and a regular material is reflection free. (The small reflections in the numerical results are solely due to the discretization and the truncation.)

The fact that the PML is reflection free is fundamentally different from the classical sponge absorbing-boundary method (e.g., Kosloff and Kosloff, 1986). Although the sponge absorbing-boundary method has been used widely and successfully in many applications, the boundary between a regular material and a sponge absorber is not reflection free even in the continuum limit. Indeed, consider a simple 1-D acoustic case with a constant density ρ and constant acoustic velocity c. At the boundary between such a medium and a sponge absorber half-space with the same density and acoustic velocity, and a constant absorbing parameter γ defined by Kosloff and Kosloff (1986), it is straightforward to derive the reflection coefficient

$$R = \frac{1 - \sqrt{1 + i\dfrac{2\gamma}{\omega} - \dfrac{\gamma^2}{\omega^2}}}{1 + \sqrt{1 + i\dfrac{2\gamma}{\omega} - \dfrac{\gamma^2}{\omega^2}}},$$

which is nonzero for any nonzero real values of γ. This reflection coefficient decreases as γ decreases, which is the basis for the tapered sponge absorber in most applications. It is worthwhile to note that this particular formulation of the sponge method can be improved for the 1-D case. Indeed, as the perfectly matched condition for the 1-D case requires only the match in impedance, it is quite straightforward to design a sponge layer so that there is no reflection for the 1-D case. This improved sponge method formulation uses partial differential equations:

$$\frac{\partial p}{\partial t} + \gamma p = -\rho c^2 \frac{\partial v}{\partial x},$$
$$\frac{\partial v}{\partial t} + \gamma v = -\rho^{-1} \frac{\partial p}{\partial x},$$

where p is the pressure field, and v is the particle velocity field. An example of velocity-stress formulation for poroviscoelastic media is given in Carcione (1998). It is straightforward to show that the reflection coefficient of this sponge layer is zero because of the match in impedance between regular medium and the sponge. However, such reflection-free sponge method formulations are not possible in the multidimensional case, as is well known in seismic modeling. This the major difference between the sponge method and the PML method can also be explained by the difference in the partial differential equations they solve. In particular in the frequency domain, for the special 2-D acoustic case, the sponge method solves (Kosloff and Kosloff, 1986)

$$\rho c^2 \left[\frac{\partial}{\partial x} \frac{1}{\rho} \frac{\partial p}{\partial x} + \frac{\partial}{\partial y} \frac{1}{\rho} \frac{\partial p}{\partial y} \right] = (-\omega^2 + \gamma^2 - i2\omega\gamma) p,$$

whereas the PML method solves

$$\rho c^2 \left[\frac{1}{e_x} \frac{\partial}{\partial x} \frac{1}{\rho e_x} \frac{\partial p}{\partial x} + \frac{1}{e_y} \frac{\partial}{\partial y} \frac{1}{\rho e_y} \frac{\partial p}{\partial y} \right] = -\omega^2 p,$$

where e_x and e_y are given by equation (7). Obviously, the anisotropic nature of the attenuation factors (i.e., different ω_x and ω_y) is present in the PML method, but not in the sponge method. For the sponge method, the reader is also refered to Carcione et al. (1988).

We argue that the zero reflection coefficient of the PML interface allows a larger attenuation factor in the PML absorber, and thus a more effective absorbing boundary than the classical sponge absorber. Along with this advantage comes the additional cost in terms of the computer memory requirement in the PML formulation. Specifically, within this PML formulation there are 12 split field variables instead of the original

four field variables. Fortunately, this increase in the memory is necessary only within the PML cells surrounding the interested domain and is quite negligible for large-scale problems.

NUMERICAL EXAMPLES

We have implemented the finite-difference algorithm with the perfectly matched layers as an absorbing boundary condition for Biot's equations in two-dimensional porous media. Unlike the continuous case, a small reflection will occur at the PML interface due to the discretization and truncation. This reflection is proportional to the contrast in the coordinate-stretching variables. Therefore, to minimize the reflection from the PML region, we use a quadratic profile with 20 cells of perfectly matched layers at the computational edge.

In the following examples, a line, pure compressional source is used to excite the seismic wave field. The source time function is the first derivative of the Gaussian function:

$$S(t) = (t - t_0)e^{-[\pi f_0(t-t_0)]^2},$$

where f_0 is the dominant frequency, and t_0 is the central time of the wavelet.

A bulk source is used in this paper. The source energy is partitioned linearly between the solid and the fluid phases:

$$W_f = \phi,$$
$$W_s = (1 - \phi),$$

where W_f is the weighting factor for the fluid motion, and W_s is for the solid motion.

A homogeneous model

A homogeneous model is used to test the effectiveness of the PML ABC. The material properties of the model are listed in Table 1. The size of the model is $N_x \times N_z = 200 \times 200$ nodes with 20 cells of PML on each side of the computational domain.

Table 1. Material and Biot's parameters for a homogeneous porous medium (from Özdenvar and McMechan, 1997).

Solid	
Bulk modulus K_s (Pa)	3.5×10^{10}
Density ρ_s (kg/m^3)	2650.0
Matrix	
Bulk modulus K_b (Pa)	4.17×10^9
Shear modulus μ (Pa)	1.855×10^9
Density (with fluid) ρ (kg/m^3)	2167.0
Porosity ϕ	0.3
Permeability κ (m^2)	1.0×10^{-12}
Tortuosity a	2.0
Fluid	
Bulk modulus K_f (Pa)	2.4×10^9
Density ρ_f (kg/m^3)	1040.0
Viscosity η (Pa s)	1.0×10^{-3}
Biot's parameters	
P (N/m^2)	9.02×10^9
Q (N/m^2)	1.23×10^9
R (N/m^2)	6.35×10^8
Seismic characteristics	
Velocity of fast P-wave (m/s)	2365
Velocity of slow P-wave (m/s)	775
Velocity of S-wave (m/s)	960

The spatial and temporal steps are $\triangle x = \triangle z = 1.5$ m and $\triangle t = 0.0001$ s. A line monopole source with a dominant frequency of 40 Hz is located at the center of the model. To inspect the reflection from the PML interface, we put one array of receivers along a vertical line running through the source.

The waveforms of vertical displacement in solid at nine locations are shown in Figure 1. In this figure, a reference result without reflection is also shown. This reference result is obtained from a much larger model with Dirichlet boundary in which reflections have not arrived within the time window of interest. Note that the results are normalized with respect to the peak value of the field at the first receiver. Because the fluid is viscous, the slow P-wave is rapidly attenuated as it propagates. We observe no obvious reflections in these waveforms.

Figure 2 shows snapshots of the vertical components of the displacement of the solid at 0.04, 0.06, 0.1, and 0.13 s when the damping coefficient b has the realistic value of 10^8N s/m^4. In this case the slow wave is diffusive and appears as a static mode at the source location (Zhang, 1999).

From the above results, it is seen that the PML method provides an effective attenuation to outgoing waves. Numerical experiments also demonstrate that this method is stable as long as $\triangle t \leq \min(\triangle x, \triangle z)/\sqrt{2}V_{\max}$ when the damping coefficient b is small. It is also noted that in this example the ratio of V_f/V_s is 2.46, which is much greater than 2 allowed in other conventional absorbing boundary conditions. We calculated the wave field with Clayton-Engquist (CE) absorbing boundary condition on the same model, and found the method becomes unstable after about 2000 time steps.

A two-layer model

In order to demonstrate the behavior of this algorithm for inhomogeneous media, we test the PML absorbing boundary condition on a two-layer model. In contrast to the homogeneous model, multiwave phases (such as reflected, transmitted, and converted phases) will be present. Some of them are relatively weak compared to the direct wave phases and are very vulnerable to the artificial reflections from the boundaries. Thus, whether these weak wave arrivals can be distinguished

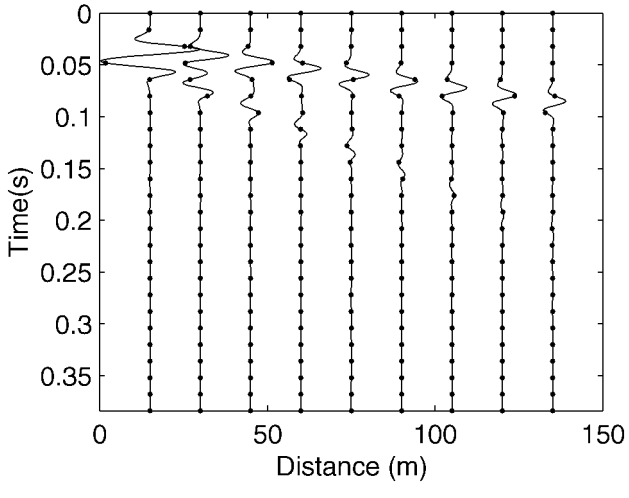

FIG. 1. Waveforms of vertical component of the solid displacement at nine vertical locations. Solid line: results from the model with PML. Dots: results with reflection.

determines the effectiveness of the absorbing boundary condition. In this example, we compare the numerical results using PML ABC with those of CE ABC. The geometry of the model is shown in Figure 3. A line monopole source is located at the center of the model which is in the upper layer. The model parameters are shown in Table 2.

The snapshot in Figure 4a at $t = 0.055$ s shows that the solid and fluid particle displacements are in phase for fast P-wave and out of phase for slow P-wave, and the fast P-wave begins to hit the interface. At $t = 0.085$ s (Figure 4b), transmitted and reflected wave phases are produced from the fast P-wave. At $t = 0.12$ s (Figure 4c), the slow P-wave reaches the interface and produces reflected and transmitted wave phases. Figure 4d shows the wave field at $t = 0.18$ s. In this figure, a very small reflection occurs from the edge.

Table 2. Material parameters for a two-layer model of porous media.

Material properties	Layer 1	Layer 2
Solid		
Bulk modulus K_s (Pa)	3.9×10^{10}	5.2×10^9
Shear modulus μ (Pa)	5.25×10^9	2.4×10^9
Density ρ_s (kg/m^3)	2588.0	2250.0
Matrix		
Bulk modulus K_b (Pa)	4.12×10^9	2.2×10^9
Density (with fluid) ρ (kg/m^3)	2167.0	2167.0
Porosity ϕ	0.25	0.1
Tortuosity a	2.49	2.42
Fluid		
Bulk modulus K_f (Pa)	2.21×10^9	2.25×10^9
Density ρ_f (kg/m^3)	952.4	1040.0
η/κ		
Damping coefficient b (N s/m^4)	3.38×10^5	3.33×10^6

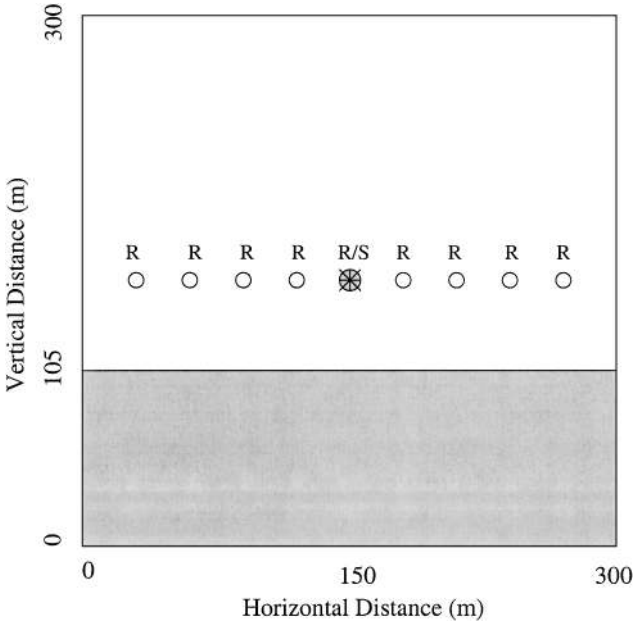

FIG. 3. Configuration of the two-layer model. R: receiver, S: source.

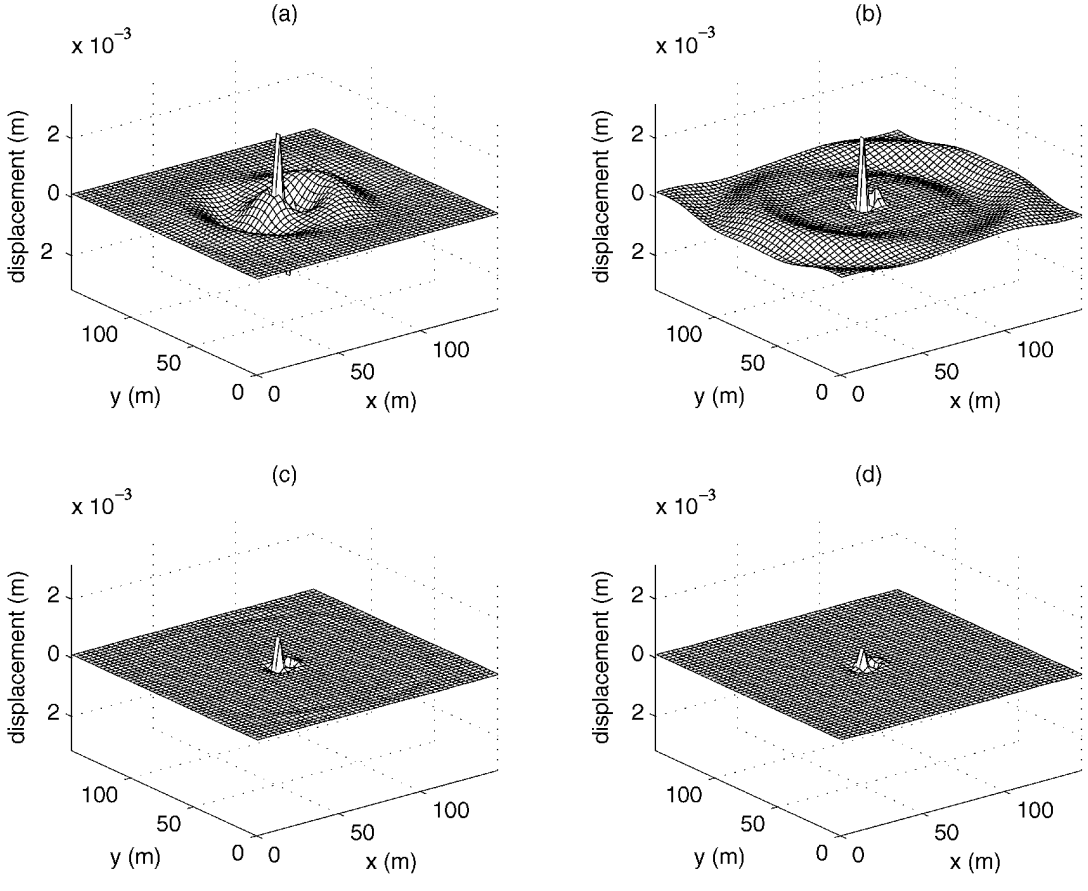

FIG. 2. Snapshots of the vertical components of the solid displacement at 0.04 s (a), 0.06 s (b), 0.1 s (c), and 0.13 s (d). The model parameters are shown in Table 1 except $b = 10^8$N s/m. A line monopole source is used.

In Figures 5 and 6, we present the synthetic seismograms for this model. The receivers are located along the line running through the source and parallel to the interface. The results from the algorithm with PML ABC are shown in Figure 5, those with CE ABC are shown in Figure 6. In order to compare the PML ABC with CE ABC, two snapshots from the method with CE ABC and two from the method with PML ABC are shown together in Figure 7. Clearly, the PML ABC has a far better performance.

CONCLUSIONS

A finite-difference method combined with the perfectly matched layer (PML) absorbing boundary condition is developed for modeling seismic wave propagation in poroelastic media. Within the boundary region of the computational domain, perfectly matched layers are used to attenuate outgoing seismic waves. The numerical results show that the outgoing waves are effectively absorbed and the reflection is very small. In contrast to some other existing absorbing boundary conditions, this new absorbing boundary condition is stable even when the ratio of the *P*-wave velocity to *S*-wave velocity is much greater than 2. Furthermore, since the PML boundary condition is directly incorporated into the wave equations, it can be used in the pseudospectral method.

ACKNOWLEDGMENT

This work is supported in parts by the Army Research Office under Grant DAAH04-96-1-0448 (Demining MURI), by the U.S. EPA under a PECASE grant CR-825-225-010, by the

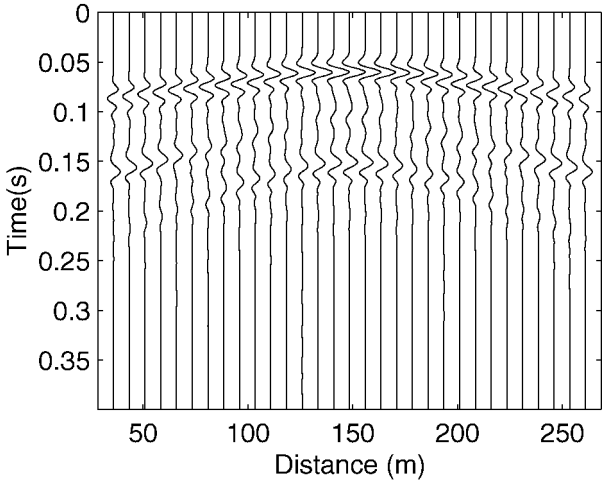

FIG. 5. Waveforms of vertical component of the solid displacement from the two-layer model with PML boundary conditions.

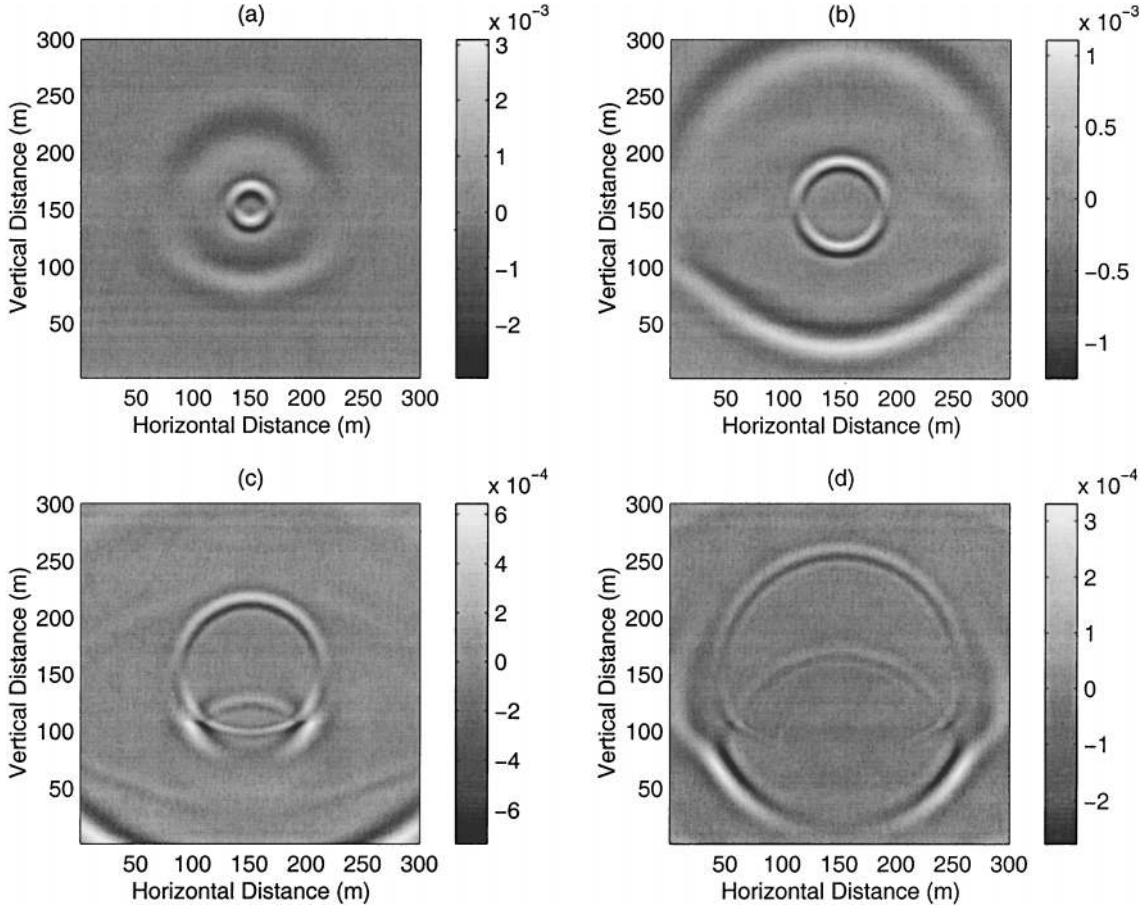

FIG. 4. Snapshots of the vertical component of the solid displacement at four different times 0.055 s (a), 0.085 s (b), 0.12 s (c), and 0.18 s (d) from the finite-difference solutions with PML. The model parameters are shown in Table 2. A monopole line source is used.

NSF under a CAREER grant ECS-9702195. The authors thank the Associate Editor and two anonymous reviewers for their suggestions to improve the manuscript.

REFERENCES

Berenger, J. P., 1994, A perfectly matched layer for absorption of electromagnetic waves: J. Comput. Phys., **114**, 185–200.

Biot, M. A., 1956a, Theory of propagation of elastic waves in a fluid-saturated porous solid. 1. Low-frequency range: J. Acoust. Soc. Am., **28**, 168–178.

———1956b, Theory of propagation of elastic waves in a fluid-saturated porous solid. 1. Higher-frequency range: J. Acoust. Soc. Am., **28**, 179–191.

———1962a, Mechanics deformation and acoustic propagation in porous media: J. Appl. Phys., **33**, 1482–1498.

———1962b, Generalized theory of acoustic propagation in porous dissipative media: J. Acoust. Soc. Am., **34**, 1254–1264.

Carcione, J. M., 1998, Viscoelastic effective rheologies for modelling wave propagation in porous media: Geophys. Prosp., **46**, 249–270.

Carcione, J. M., Kosloff, D., and Kosloff, R., 1988, Viscoacoustic wave propagation simulation in the earth: Geophysics, **53**, 769–777.

Cerjan, C., Kosloff, D., Kosloff, R., and Reshef, M., 1985, A nonreflecting boundary condition for discrete acoustic and elastic wave equations: Geophysics, **50**, 705–708.

Chew, W. C., and Liu, Q. H., 1996, Perfectly matched layers for elastodynamics: A new absorbing boundary condition: J. Comp. Acoust., **4**, no. 4, 72–79.

Chew, W. C., and Weedon, W. H., 1994, A 3-D perfectly matched medium from modified Maxwell's equations with stretched coordinates: Microw. Opt. Technol. Lett., **7**, 599–604.

Clayton, R., and Engquist, B., 1977, Absorbing boundary conditions for acoustic and elastic wave equations: Bull. Seism. Soc. Am., **67**, 1529–1540.

Hastings, F. D., Schneider, J. B., and Broschat, S. L., 1996, Application of the perfectly matched layer (PML) absorbing boundary condition to elastic wave propagation: J. Acoust. Soc. Am., **100**, 3061–3069.

He, J., and Liu, Q. H., 1999, A nonuniform cylindrical FDTD algorithm with improved PML and quasi-PML absorbing boundary conditions: IEEE Trans. Geosci. Remote Sensing, **37**, 1066–1072.

Kosloff, R., and Kosloff, D., 1986, Absorbing boundary for wave propagation problems: J. Comp. Phys., **63**, 363–376.

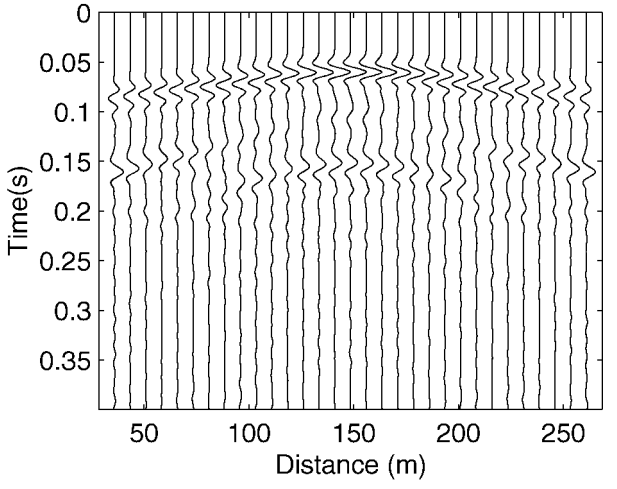

FIG. 6. Waveforms of vertical component of the solid displacement from the two-layer model with CE boundary conditions.

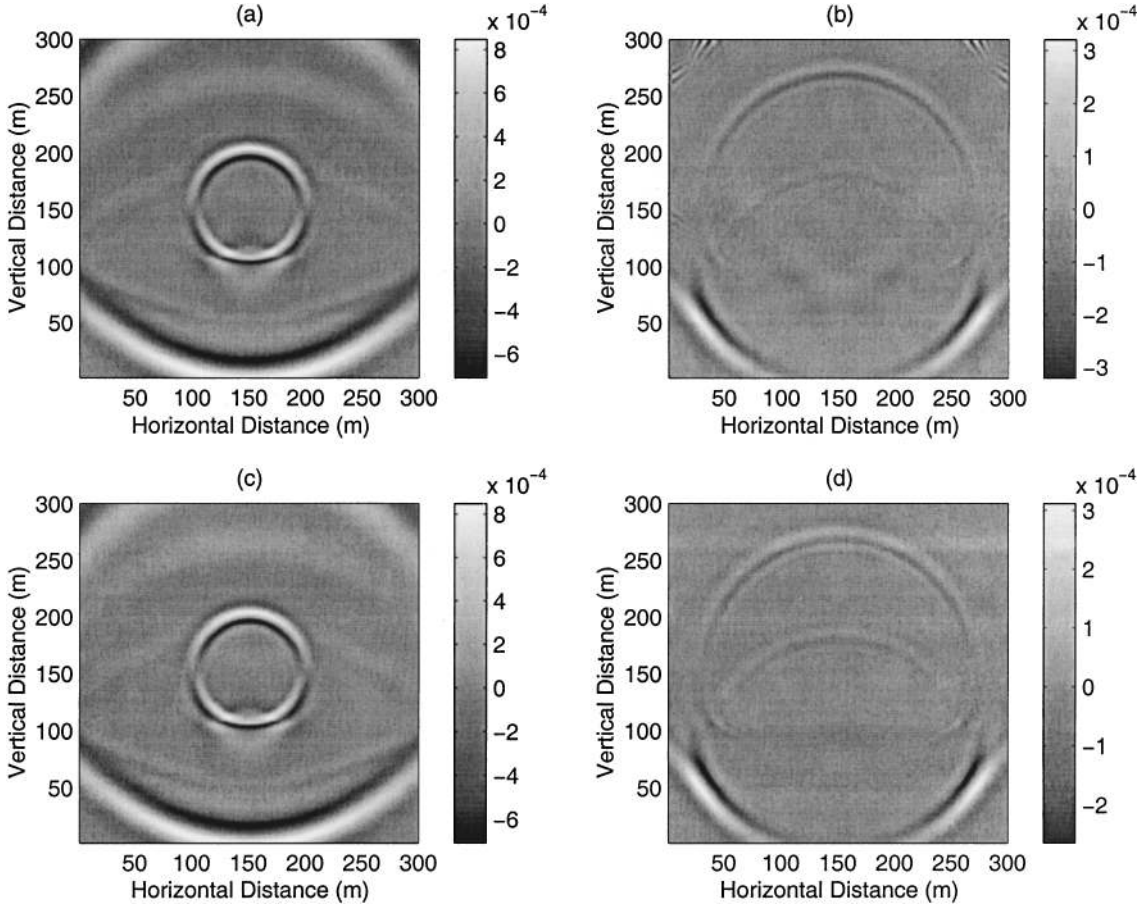

FIG. 7. Snapshots at times 0.1 s (a) and 0.2 s (b) for a two-layer model from the method with CE ABC. Snapshots at times 0.1 s (c) and 0.2 s (d) for the same model from the method with PML ABC. The model parameters are shown in Table 2 . A monopole line source is used.

Liao, Z. P., Wong, H. L., Yang, B. P., and Yuan, Y. F., 1984, A transmitting boundary for transient wave analysis: Sci. Sinica A, **27**, 1063–1076.

Liu, Q. H., 1997, An FDTD algorithm with perfectly matched layers for conductive media: Microw. Opt. Technol. Lett., **14**, 134–137.

———1998, The PSTD algorithm for acoustic waves in inhomogeneous, absorptive media: IEEE Trans. Ultrason., Ferroelect., Freq. Contr., **45**, 1044–1055.

———1999, Perfectly matched layers for elastic waves in cylindrical and spherical coordinates: J. Acoust. Soc. Am., **105**, 2075–2084.

Liu, Q. H. and Tao J., 1997, The perfectly matched layer for acoustic waves in absorptive media: J. Acoust. Soc. Am., **102**, 2072–2082.

Mahrer, K. D., 1986, An empirical study of instability and improvement of absorbing boundary conditions for elastic wave equation: Geophysics, **51**, 1499–1501.

Özdenvar, T., and McMechan, G. A., 1997, Algorithm for staggered-grid computations for poroelastic, elastic, acoustic, and scalar wave equations: Geophys. Prosp., **45**, 403–420.

Reynolds, A. C., 1978, Boundary conditions for the numerical solution of wave propagation problems: Geophysics, **43**, 1099–1110.

Smith, W. D., 1974, A nonreflecting plane boundary for wave propagation problems: J. Comp. Phys., **15**, 492–503.

Stacey, R., 1988, Improved transparent boundary formulations for the elastic-wave equation: Bull. Seism. Soc. Am., **78**, 2089–2097.

Teixeira, F. L., and Chew, W. C., 1997, PML-FDTD in cylindrical and spherical coordinates: IEEE Microwave Guided Wave Lett., **7**, 285–287.

Zhang, J., 1999, Quadrangle-grid velocity-stress finite-difference method for poroelastic wave equations: Geophys. J. Internat., **139**, 171–182.